Supplementary Information

Amino-Functionalized Nitrogen-Doped Graphene Quantum Dots for Efficient Enhancement of Two-Photon-Excitation Photodynamic Therapy: Functionalized Nitrogen as a Bactericidal and Contrast Agent

Wen-Shuo Kuo[1,2#], Tien-Sung Yeh[3#], Chia-Yuan Chang[4], Jui-Chang Liu[2], Chang-Hsin Chen[5], Edmund Cheung So[6,7], and Ping-Ching Wu[8*]*

[1]School of Chemistry and Materials Science, Nanjing University of Information Science and Technology, Nanjing 210044, Jiangsu, China
[2]Allergy & Clinical Immunology Research Center, National Cheng Kung University Hospital, College of Medicine, National Cheng Kung University, Tainan 701, Taiwan (R.O.C.)
[3]Department of Physical Medicine and Rehabilitation, An Nan Hospital, China Medical University, Tainan 709, Taiwan (R.O.C.)
[4]Department of Mechanical Engineering, National Cheng Kung University, Tainan 701, Taiwan (R.O.C.)
[5]AbVision Inc., CA, 95035 USA
[6]Department of Anesthesia & Medical Research, An Nan Hospital, China Medical University, Tainan 709, Taiwan (R.O.C.)
[7]Graduate Institute of Medical Science, Chang Jung Christian University, Tainan 711, Taiwan (R.O.C.)
[8]Department of Biomedical Engineering, National Cheng Kung University, Tainan 701, Taiwan (R.O.C.)
[#] The authors contributed equally to this work.

*To whom correspondence should be addressed. E-mail: edmundsotw@gmail.com (E.-C.S.); wbcxyz@bme.ncku.edu.tw (P.-C. W.)

Materials and Methods

Preparation of amino-N-GQDs[1-3]

GQDs. Graphene oxide was prepared from a natural graphite powder (Bay carbon Inc., Bay City, MI, USA) using a modified Hummers' method. Graphite (8.5 M) and $NaNO_3$ (0.6 M) (Merck & Co., Kenilworth, NJ, USA) were mixed with H_2SO_4 (Sigma Aldrich Co., St Louis, MO, USA). $KMnO_4$ (2.0 M) (FUJIFILM Wako Chemicals USA Inc., Richmond, VA, USA) was slowly added with continual stirring at 35 °C overnight. Subsequently, deionized water (ddH_2O) was gradually added and continually stirred. H_2O_2 (Sigma Aldrich Co., St Louis, MO, USA) was added to terminate the reaction. Washing and centrifugation with ddH_2O were performed several times, and the graphene oxide was collected. The as-prepared graphene oxide was placed in a tube furnace and heated to 400–600 °C in the presence of argon for 4–6 h; it was subsequently introduced to concentrated HNO_3 (16.0 M) (Sigma Aldrich Co., St Louis, MO, USA) and stirred for 2 d. The mixture was placed in a sonicator for 2 d and subsequently placed in an oven at 160 °C for 1 d to vaporize all the liquid. Washing and centrifugation (83000 rpm; Optima TLX Ultracentrifuge, Optima TLX Ultracentrifuge, Beckman Coulter Inc., Danville, CA, USA) with ddH_2O were conducted several times. The supernatant was filtered through a 0.22 μm microporous membrane. The pH of the resulting black suspension was tuned to 7.4 with NaOH, and GQDs were obtained. *N-GQDs.* Graphene oxide was prepared from a natural graphite powder (Bay carbon, SP-1) using a modified Hummers' method. Graphite (8.5 M) and $NaNO_3$ (0.6 M) were mixed with H_2SO_4. $KMnO_4$ (2.0 M) was slowly added with continual stirring at 35 °C overnight. Subsequently, ddH_2O was gradually added and continually stirred. H_2O_2 was added to terminate the reaction. Washing and centrifugation with ddH_2O were performed several times, and the graphene oxide was collected. The as-prepared graphene oxide was placed in a tube furnace and heated to 400–600 °C in the presence of ammonia for 4–6 h; it was subsequently introduced to concentrated HNO_3 (16.0 M) and stirred for 2 d. The mixture was placed in a sonicator for 2 d and subsequently placed in an oven at 160 °C for 1 d to vaporize all the liquid. Washing and centrifugation (83000 rpm) with ddH_2O were conducted several times. The supernatant was filtered through a 0.22 μm microporous membrane. The pH of the resulting black suspension was tuned to 7.4 with NaOH, and N-GQDs were obtained. *Amino-N-GQDs.* Graphene oxide was prepared from a natural graphite powder (Bay carbon, SP-1) using a modified Hummers' method. Graphite (8.5 M) and $NaNO_3$ (0.6 M) were mixed with H_2SO_4. $KMnO_4$ (2.0 M) was slowly added with continual stirring at 35 °C overnight. Subsequently, ddH_2O was gradually added and continually stirred. H_2O_2 was added to terminate the reaction. Washing and centrifugation with ddH_2O were performed several times, and the graphene oxide was collected. The as-prepared graphene oxide was placed in a tube furnace and heated to 400–600 °C in the presence of ammonia for 4–6 h; it was subsequently introduced to concentrated HNO_3 (16.0 M) and stirred for 2 d. The mixture was placed in a sonicator for 2 d and subsequently placed in an oven at 160 °C for 1 d to vaporize all the liquid. Washing and centrifugation (83000 rpm) with ddH_2O were conducted several times. The supernatant was filtered through a 0.22 μm microporous membrane. The pH of the resulting black suspension was tuned to 7.4 with NaOH, and N-GQDs were obtained. Then, N-GQDs were mixed with ammonia, stored in a

Teflon-lined stainless steel autoclave, and reacted at 180 °C for 5 h. The resulting mixture was washed with ddH_2O, centrifuged several times, and subsequently dried in an oven at 50 °C overnight. Eventually, amino-N-GQDs were obtained (Scheme S1A).

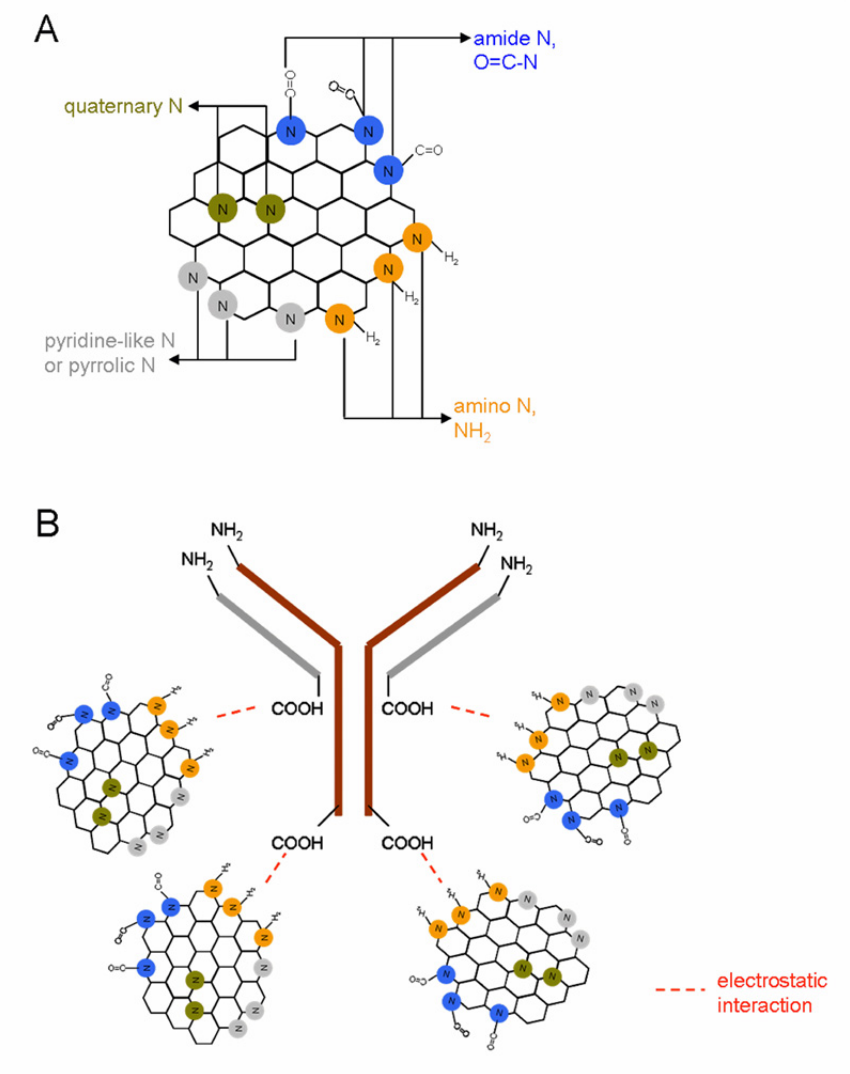

Scheme S1. The conceptual schemes of (**A**) the amino-N-GQD and (**B**) the amino-N-GQD-Ab.

Characterization

Materials were subject to transmission electron microscopy (TEM, JEOL 2100F and JEOL 3010, Akishima, Tokyo, Japan) observation. The height profile diagram, thickness and size of samples were determined by Atomic force microscopy (AFM, multimode 8, Bruker, Billerica, MA, USA). Fourier-transform infrared spectroscopy (FTIR), Ultraviolet-visible (UV-vis) spectroscopy, X-ray diffraction (XRD) and zeta potential spectra of samples were recorded by the spectrometers: RX1, PerkinElmer, Waltham, MA, USA; U-4100 Hitachi, Chiyoda-ku, Tokyo; Bruker AXS Gmbh, D2 Phaser, Billerica, MA, USA; and Malvern Nano-ZS90, Worcestershire, West Midlands, UK, respectively. Raman spectroscopy (DXR, Thermo Scientific, Waltham, MA, USA) was used to examine the crystallinity of samples with 532 nm laser. X-ray photoelectron spectroscopy (XPS, PHI 5000, VersaProbe, Chanhassen,

MN, USA) was employed to examine the surface chemistry of the materials, the O(1s)/C(1s) and N(1s)/C(1s) atomic ratios of materials. The PL signal was recorded by the spectrophotometer (F-7000, Hitachi, Chiyoda-ku, Tokyo, Japan).

Bacterial cultures

Bacillus subtilis (*B. subtilis*) obtained from our own laboratory were grown in nutrient agar of Luria-Bertani (LB) broth (per liter: tryptone 10g, yeast extract 5g, sodium chloride 10g, agar 15g, and pH tuned to 7.5) (Sigma Aldrich Co., St Louis, MO, USA) and incubated at 37 °C.

Coating antibody

The absorbance of a certain quantity of antibody [anti-TasA antibody (Ab_{TasA}) (abcam, Cambridge, UK) was recorded via UV-vis spectroscopy (Abs: approximately 203 nm)]. By the electrostatic interaction, the materials were mixed with the same quantity antibody for 30 min of incubation at 4 ℃ in the dark and centrifuged (83000 rpm) to remove excess antibody; the material-Ab_{TasA} was then prepared. Conversely, the supernatant was retained and its absorbance was measured. The difference between the absorbance of the collected supernatant and the original antibody was estimated (Figure S10). Consequentially, the quantity of the antibody absorbed on the materials was calculated using Lambert-Beer's law [A= εbC, where A= absorbance, ε= molar extinction coefficient, b= path length (1 cm), and C= concentration]. In the working solution of 1×PBS buffer, there was approximately 0.14 μg of Ab_{TasA} absorbed on 1 μg of amino-N-GQD. This implies that the absorption efficiency of 1×PBS buffer was approximately 14.0% (zeta potential of amino-N-GQD-Ab_{TasA}: 16.3 mV), and was 13.8% (16.0 mV of zeta potential) in culture medium of *B. subtilis* (Scheme S1B). For N-GQD-Ab_{TasA} and GQD-Ab_{TasA}, the efficiency of absorption was approximately 12.6% (15.2 mV of zeta potential) and 11.4% (10.2 mV of zeta potential) in 1×PBS buffer, 13.0% (15.4 mV of zeta potential) and 11.7% (10.6 mV of zeta potential) in culture medium of *B. subtilis*. Since there is not much different between the zeta potential of material-Ab in 1×PBS buffer and culture mediums, it meant that the biomolecules would be absorbed on neither material and Ab nor material-Ab. In other words, the interaction among Ab, material-Ab and bacteria would not be influenced by biomolecules in cultural mediums, leading to no subsequently effect in the specific binding between them. Additionally, the positively charged material-Ab was favorable for absorbance or internalization by the negatively charged bacterial surface. The above results have proven the successful absorption of Ab on the surface of materials (Table S6).

Biocompatibility assay with colony forming unit (CFU) counting method

B. subtilis (OD_{600} ~0.05) was added with material-Ab_{TasA} (6 μg mL^{-1}) by incubating for 3 h at 37 °C. After incubation, the mixture was centrifuged and the pellets of bacteria were diluted (OD_{600} ~0.05). Then, a dilution factor in the range of 10^{-5} to 10^{-8} was used for the incubated bacteria with plating on the agar plates. The plates were placed overnight in an incubator at 37 °C. The number of surviving bacteria was determined and expressed as a percentage (%) that corresponds to the unit of CFU mL^{-1} after incubation. Data are means ± SD (n=6)

Quantum yield (QY) measurement[4]

The relative PL QY of contrast agent is usually the ratio of the emitted photons to the absorbed photons and is given as follows:

$$QY = QY_{ref}\left(\eta^2/\eta_{ref}^2\right)(I/A)\left(A_{ref}/I_{ref}\right) \quad \text{(S1)}$$

, where QY_{ref} =0.28 is the QY of Cy5.5 dissolved in dimethyl sulfoxide (DMSO; Fisher Scientific, Hampton, NH, USA) as a reference, η is the refractive index of ddH_2O=1.33 (η_{ref} of DMSO=1.48), I is the integrated fluorescence intensity and A is the absorbance at the excitation wavelength. One-photon excitation (OPE) or TPE yields the same QY.

Singlet oxygen QY (ψ_Δ) measurement[5]

From previous studies, ψ_Δ can be obtained. ψ_Δ measurements were conducted in D_2O at 355 nm by using *meso*-tetra(4-sulfonatophenyl)porphine dihydrochloride (Sigma-Aldrich, St. Louis, MO, USA) as a reference (ψ_Δ= 0.64).

Femtosecond laser optical system for the measurements of two-photon absorption (TPA) and TPL[2]

The home-made femtosecond titanium-sapphire (ti-sa) laser optical system (a repetition rate of 80 MHz; Tsunami, Spectra-Physics, Santa Clara, CA, USA) was used according to the previous studies. <u>*TPA measurement.*</u> With 2 m ms^{-1} speed of the galvanometer scanner, the excitation spectrum was measured as 720-820 nm with an excitation power of 2.8 mW [this is the power before objective; the power after objective (or on sample) is 0.9856 mW or 98.56 nJ $pixel^{-1}$)]. Therefore, the relative TPA spectrum as function of excitation wavelength for the material was measured. <u>*Measurement of TPL spectrum.*</u> The material was exposed to TPE from the femtosecond laser at an excitation wavelength of 800 nm, a power of 98.56 nJ $pixel^{-1}$ (0.9856 mW), a scanning area of 200 μm × 200 μm, a frequency of 10 kHz, an exposure time of 1.638 s/(scan, pixel)= 100 μs, 128 × 128 pixels $scan^{-1}$, and a pixel area of 1562.5 nm × 1562.5 nm. The focal spot area was calculated as $\pi d^2/4$, where d = 0.61 λ/numerical aperture (*NA*) is the full width at half maximum of the beam waist. For instance, at the *x*–*y* axis focal spot with 800 nm excitation and a 40× oil-immersion objective with an *NA* of 1.3, d = 0.61 × 800 nm/1.3 = 375.38 nm= 0.37538 μm, and the *z*-axis resolution was measured to be 0.90265 μm (Figure 1). For 800 nm excitation, the exposure time per scan for an individual material is expressed as (focal spot area/pixel area) × 100 = 4.53 ms, and the total exposure time t = 4.53 ms × number of scans. A 40× oil-immersion objective (*NA* 1.3) was used to collect the signals, and the detection range of the spectrum photometer was 300-695 nm in wavelength.

The calculations of laser power (mW or nJ $pixel^{-1}$) used on the sample were as follows. For the 40× oil-immersion objective (*NA* 1.3), the transmission rate at 800 nm in wavelength is approximately 88% in this optical system, and the laser power went from the output to the objective with only 40% of the original output power due to the loss of power. As a result, the calculated energy after the objective (on sample) is P_{output} (mW)*40%*88%= 0.352*P_{output} (mW). For instance, P_{output} = 3.0 mW, the calculated energy after the objective (on the sample) is 3.0 mW*40%*88%= 1.056 mW. With 10 kHz of scan rate (each pulse stays 0.1 ms $pixel^{-1}$), the calculated energy on the sample (J $pixel^{-1}$) was around P_{output} (mW)*40%*88%*0.1 ms= 0.0352*P_{output} (J $pixel^{-1}$). For instance, P_{output} = 3.0 mW, the energy (J $pixel^{-1}$)

on sample= 3.0 mW*40%*88%*0.1 ms= 0.1056 μJ pixel^{-1}= 105.6 nJ pixel^{-1} (nJ pixel^{-1}). The power after the objective (on the sample) was used and marked throughput this manuscript.

Measurement of TPE absolute cross section[6,7]

The absolute cross section of TPE was measured the luminescence signal *via* femtosecond laser optical system according to previous studies. The TPL of fluorescein and rhodamine B (Sigma Aldrich Co., St. Louis, MO, USA) had to be verified. The results are shown in Figure 5c and were obtained by measuring the dependence of the emission intensity with an excitation power range of 704.00 nJ pixel^{-1} (7.04 mW) to 2816.00 nJ pixel^{-1} (28.16 mW). Quadratic dependence with the exponents of approximately 2.00 for fluorescein and approximately 1.99 for rhodamine B was measured for increasing the excitation power to determine the luminescence from TPE. According to the previous studies, the action cross sections of TPE for fluorescein and rhodamine B are 36.4 and 153.0 Göeppert–Mayer units (GM; 1 GM = 10^{-50} cm^{4}s photon^{-1}), respectively, for 800 nm excitation. We also referred to the free website http://www.drbio.cornell.edu/cross_sections.html, kindly provided by Prof. Chris Xu (Cornell University, NY, USA). The TPE action cross sections for fluorescein and rhodamine B were calculated to be 35.8 and 154.2 GM, respectively, which indicated an error of less than 5% compared with those from Prof. Xu's laboratory. In this study, rhodamine B was chosen as the standard reference for determining the cross section, and the calculated absolute cross sections of TPE for the amino-N-GQD, N-GQD and GQD were approximately 54,012.73 GM, 51,627.52 GM and 48,378.98 GM, respectively. The measured parameters for calculating the TPE absolute cross sections of samples are shown in Table 1. No batch-to-batch variation was observed for the material in two-photon properties, two-photon photodynamic ability, and two-photon contrast agents.

Femtosecond laser optical system (for fluorescence lifetime imaging microscopy, FLIM)[7]

The home-made femtosecond titanium-sapphire (ti-sa) laser optical system (repetition rate of 80 MHz; Tsunami, Spectra-Physics, Santa Clara, CA, USA) was used according to the previous studies. The lifetime data and the parameter generated using the triple-exponential equation fitting while monitoring the emission under TPE (Ex: 800 nm).

Calculation of radiative and non-radiative decay rates[2]

PL QY and lifetime are both major parameters when investigating the emission characteristics of fluorescent dyes in diverse environments. The quantum yield (Q) can be expressed as follows:

$$Q = \frac{\Gamma}{\Gamma + \mathrm{k}} \tag{S2}$$

, where Γ is the radiative decay rate and *k* is the nonradiative decay rate. Fluorescence lifetime is usually defined as the average time required for an electron in the excited state to decay to the ground state. The TPL lifetime τ can also be relative to the decay rates and is described as follows:

$$\tau = \frac{1}{\Gamma + \mathrm{k}} \tag{S3}$$

Following Eqs. (S2-S3), the radiative and nonradiative decay rates can be calculated.

ROS detection[2,8-10]

Singlet oxygen ($^1O_2$). (a) Material-Ab (6 μg mL^{-1}) was treated with *B. subtilis* (OD_{600} ~0.05), after which it was subjected to 3 h of incubation at 37 °C in darkness. Subsequently, the mixture was exposed to TPE photoexcitation (394.24 nJ $pixel^{-1}$, 700 scans; Ex: 800 nm) and finally mixed with Singlet Oxygen Sensor Green (SOSG) reagent (1 μM; Thermo Fisher Scientific, Waltham, MA, USA) (Ex/Em: 488/525 nm). A fluorescence spectrometer was employed for measurements. For ROS neutralization, the mixture was mixed with 30 ppm of antioxidant *α*-tocopherol/methyl linoleate (Sigma-Aldrich, St. Louis, MO, USA) in darkness and exposed to TPE photoexcitation with the same treatment. (b) Material-Ab (6 μg mL^{-1}) was treated with *B. subtilis* (OD_{600} ~0.05), after which it was subjected to 3 h of incubation at 37 °C in darkness. Subsequently, the mixture was exposed to TPE photoexcitation (394.24 nJ $pixel^{-1}$, 700 scans; Ex: 800 nm) and finally mixed with 10 μM of trans-1-(2′-methoxyvinyl)pyrene (*t*-MVP, Thermo Fisher Scientific, Waltham, MA, USA)/0.10 M SDS (Sigma-Aldrich, St. Louis, MO, USA) (Ex/Em: 352/465 nm) For ROS neutralization, the mixture was mixed with 30 ppm of antioxidant *α*-tocopherol/methyl linoleate (Sigma-Aldrich, St. Louis, MO, USA) in darkness. Reaction of *t*-MVP with $^1O_2$ yields a dioxetane intermediate that fluoresces while it decomposes into 1-pyrenecarboxaldehyde. Furthermore, this highly selective fluorescent probe does not react with other activated oxygen species such as hydroxyl radicals, superoxide, or hydrogen peroxide. A fluorescence spectrometer was employed for measurements. ROS neutralization was conducted with the same as previously described treatment. *Superoxide radical anion ($O_2^{\cdot-}$).* (a) Material-Ab (6 μg mL^{-1}) was treated with *B. subtilis* (OD_{600} ~0.05), after which it was subjected to 3 h of incubation at 37 °C in darkness. Subsequently, the mixture was exposed to TPE photoexcitation (394.24 nJ $pixel^{-1}$, 700 scans; Ex: 800 nm) and finally mixed with 2,3-bis (2-methoxy-4-nitro-5-sulfophenyl)- 2H-tetrazolium-5-carboxanilide (XTT, 0.45 mM; Sigma-Aldrich, St. Louis, MO, USA). The purpose of this material was that it interacted with $O_2^{\cdot-}$ and produced XTT-formazan, resulting in strong absorption (470 nm in wavelength). UV-vis spectrometer was employed to monitor this absorption. For ROS neutralization, the mixture was mixed with 30 ppm of antioxidant *α*-tocopherol/methyl linoleate (Sigma-Aldrich, St. Louis, MO, USA) in darkness and exposed to TPE photoexcitation with the same treatment. (b) Material-Ab (6 μg mL^{-1}) was treated with *B. subtilis* (OD_{600} ~0.05), after which it was subjected to 3 h of incubation at 37 °C in darkness. Subsequently, the mixture was exposed to TPE photoexcitation (394.24 nJ $pixel^{-1}$, 700 scans; Ex: 800 nm) and finally mixed with 50 mM bicarbonate buffer (pH 8.60) and glutathione (*γ*-L-glutamyl-L-cysteinyl-glycine, GSH; Sigma-Aldrich, St. Louis, MO, USA)/0.80 mM bicarbonate buffer (the Ellman's assay for $O_2^{\cdot-}$ detection). Subsequently, the following experiments were conducted according to the procedure in a previous study. Loss of GSH (%) was calculated as the difference in absorbance between the sample and negative control divided by the absorbance of the negative control. The signal of the generated $O_2^{\cdot-}$ was obtained as described in the previous calculation. Data are means ± SD (n = 6).

Uptake assay

B. subtilis (OD_{600} ~ 0.05) were incubated with 6 μg mL^{-1} material–Ab_{TasA}. The absorbance of a quantity

of 6 μg mL^{-1} material–Ab_{TasA} was recorded using UV-vis spectroscopy (Abs: approximately 203 nm). The materials were mixed with *B. subtilis* (**OD_{600}** ~ 0.05) at 37 ℃ from 1h to 10h, respectively. Then, the mixture was centrifuged (1200 rpm) to remove excess materials, keep the supernatant, and measure the absorbance and the supernatant. The difference between the absorbance values of the collected supernatant and the original materials was estimated, thus resulting in the percentage of uptake at each time point. Data are means ± SD (n=6).

Statistical Analysis

The statistical significance was by the analysis of variance. The p-value was considered statistically significant for all the treatments.

And there is no batch to batch variation for the materials in terms of two-photo properties, and two-photon contrast agents. Different optical system has different detection depth. Due to the detection efficiency and the objective we used, the maximal z depth we can be observed by this laser optical system is approximately 100 μm. However, 99 μm in the work can show the optimal resolution in the mimic 3D biological specimens.

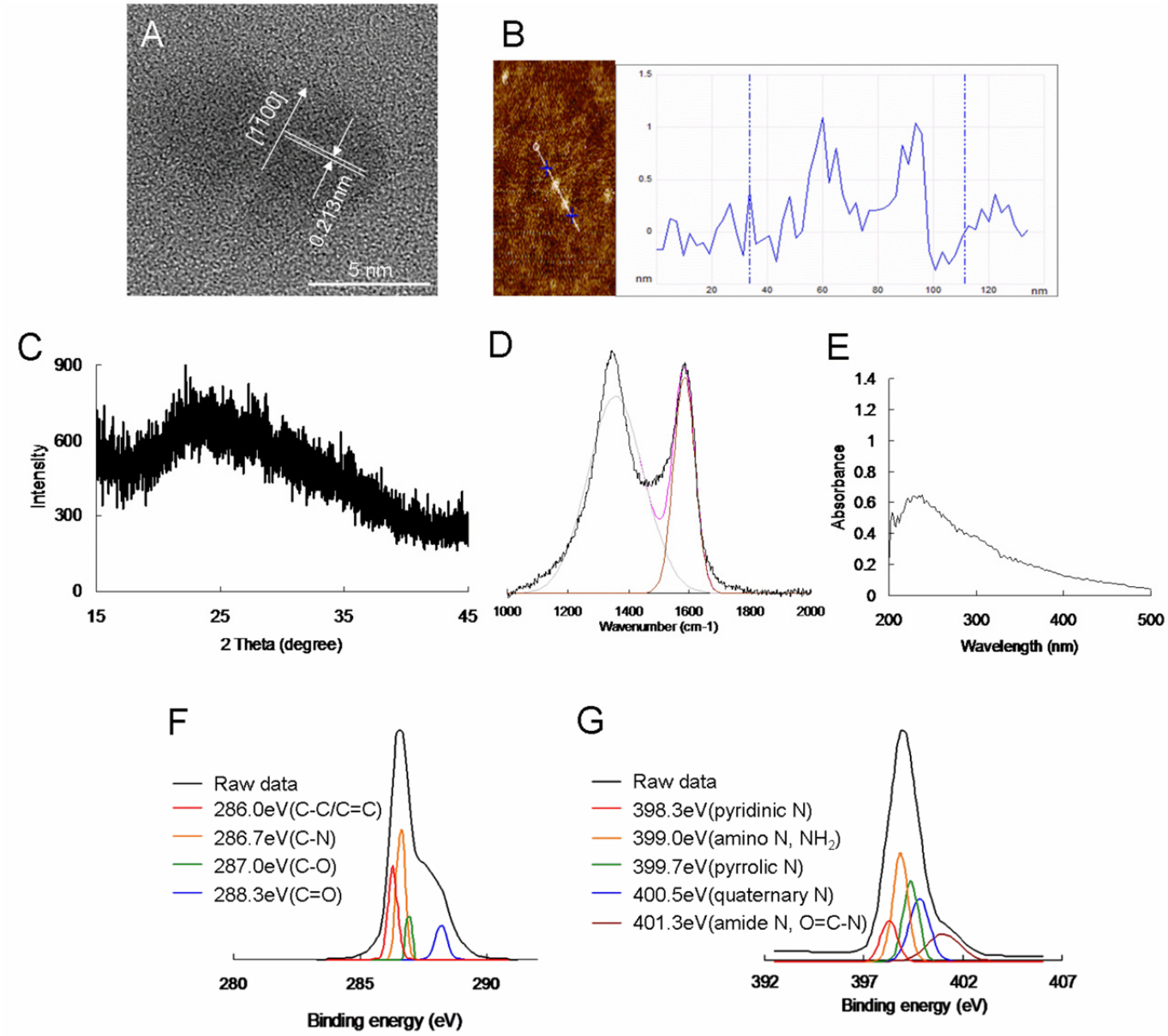

Atomic ratio O(1s)/C(1s)	Carbon bonding composition (%)			
	C-C/C=C	C-N	C-O	C=O
28.2%	30	39	13	18

N(1s)/C(1s)	Nitrogen bonding composition (%)				
	pyridinic	amino	pyrrolic	quaternary	amide
4.5%	16	28	22	20	14

Figure S1. (**A**) HR-TEM image obtained for a single amino-N-GQD, which exhibited a *d*-spacing of 0.213 nm, graphene $\{1\bar{1}00\}$ lattice planes, and a mean lateral size of 7.1 ± 0.6 nm. (**B**) AFM image of amino-N-GQDs on mica. The height difference between two arrows (the amino-N-GQDs and mica) was 1.08 ± 0.03 nm. (**C**) XRD pattern of the amino-N-GQDs. (**D**) Raman spectroscopy results indicating the material's crystallinity. The gray and brown lines indicate that the spectrum was decomposed and fitted to the D-band (~1384 cm^{-1}) and G-band (~1607 cm^{-1}) peaks (black line: raw data; pink line: decomposed spectrum). The I_D/I_G ratio was approximately 0.88. (**E**) UV–Vis spectrum of the materials (the peak at 221

nm corresponded to the π–π* transition of aromatic C=C bonds and the n–π* transitions of the C–N and C=O shoulder appeared at approximately 324 nm). (**F,G**) Peaks fitted using a Gaussian function for the deconvoluted C(1s) and N(1s) XPS spectra. The peaks of nonoxygenated rings (C–C/C=C),C–N bonds, hydroxyl group bonds (C–O), and carbonyl group bonds (C=O) were fitted using a Gaussian function for the deconvoluted C(1s) XPS spectra. The peaks of pyridinic N, amino N (NH_2), pyrrolic N, quaternary N, and amide N (O=C–N) were fitted using a Gaussian function for the deconvoluted N(1s) XPS spectra. The atomic ratios and bind compositions for the amino-N-GQDs are summarized in the table. The O(1s)/C(1s) and N(1s)/C(1s) atomic ratios were 28.2% and 4.5%, respectively. The delivered material dose was 6 μg mL^{-1}.

Table S1. Quantitative size distribution was determined by dynamic light scattering.

	Size (nm)	3.5	4.5	5.5	6.5	7.5	8.5	9.5	10.5
Amino-N-GQD	Fraction (%)	0	2	12	31	32	17	6	0
N-GQD	Fraction (%)	0	3	14	30	33	15	5	0
GQD	Fraction (%)	0	3	12	33	34	16	2	0

Raman spectroscopy was used to monitor the inelastic phonon scattering caused by the vibration of chemical bonds[11] which enables to calculate the size of the sp^2 domain in the amino-N-GQD, N-GQD and GQD, respectively. If the mean size of the GQD-based materials > 3 nm, follow the Eq. (S4),[12,13]

$$L_a\ (\text{nm}) = (2.4 \times 10^{-10})\ \lambda_{laser}^{4}\ (I_D/I_G)^{-1} \quad \text{(S4)}$$

where L_a (nm) is the mean size of the sp^2 domain; λ_{Laser} is the excitation wavelength (nm); I means the intensity for the D band and G band, respectively.

However, if the mean size of the GQD-based materials < 3 nm, follow the Eq. (S5),[14]

$$L_D = 0.54\ E_L^{4}\ (I_D/I_G) \quad \text{(S5)}$$

where is that in small-size graphene sheets with point-like defects containing sp^3-bonded carbon atoms, the mean distance between defects, L_D (nm), is generally used to represent the size of the sp^2 domains L_D, (nm); E_{Laser} is the excitation laser energy (eV) used in Raman experiments.

The Raman spectra were obtained with a 532 nm laser and were decomposed into the D band and G band by the Lorentzian function. According to the calculations based on the Eqs. (S4-S5), the diameter of the amino-N-GQD, N-GQD and GQD was 7.0 nm (compared to 7.1 ± 0.6 nm of that determined by HR-TEM), 6.8 nm (compared to 7.0 ± 0.4 nm of that determined by HR-TEM) and 6.7 nm (compared to 6.8 ± 0.5 nm of that determined by HR-TEM).

FTIR spectroscopy was used to analyze the exposed functional groups of the amino-N-GQD (**Figure S2**). The results showed characteristic bands of amino-N-GQD for N–H vibration about 845 cm^{-1} (band 1), C–O stretching about 1048 cm^{-1} (band 2), C–N stretching about 1182 cm^{-1} (band 3), N–C=O stretching about 1236 cm^{-1} (band 4), tertiary alcoholic C–OH bending about 1411cm^{-1} (band 5), C=C ring about 1679 cm^{-1} (band 6), N–H bending and amide about 1776 cm^{-1} (band 7), C=O stretching about 1845 cm^{-1} (band 8), N–H stretching about 2917 cm^{-1} (band 9), and N–H vibration about 3328 cm^{-1} (band 10).

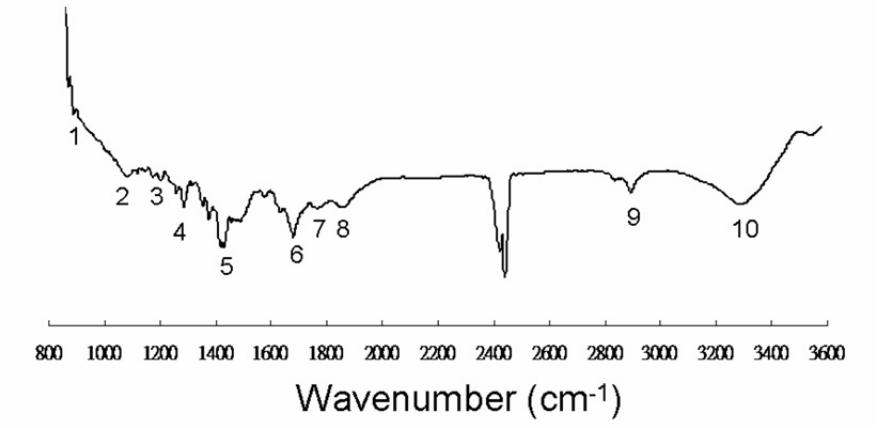

Figure S2. FTIR spectrum of amino-N-GQD.

Table S2. Amount of ROS generated, as observed by conducting TPE (394.24 nJ pixel^{-1}, 700 scans; Ex: 800 nm) on materials in the dark. The delivered dose of the materials was 6 μg mL^{-1}. Data are means ± SD (n=6).[2,8-10,15-20]

$^1O_2$ (by SOSG)[c]								
Negative control[ac]	ROS neutralization[abc]	Positive Control[cd]	amino-N-GQD	ROS neutralization[bc]	N-GQD	ROS Neutralization[bc]	GQD	ROS Neutralization[bc]
223±9	225±12	2456±122	1616±111	224±13	918±50	222±10	683±19	224±11

$^1O_2$ (by *t*-MVP)[e]								
Negative control[ae]	ROS neutralization[abe]	Positive Control[de]	amino-N-GQD	ROS neutralization[be]	N-GQD	ROS Neutralization[be]	GQD	ROS Neutralization[be]
330±22	334±21	7962±191	5015±126	332±18	3157±66	331±23	2155±58	330±19

$O_2^{\bullet-}$ (by XTT)[f]								
Negative control[af]	ROS neutralization[abf]	Positive Control[df]	amino-N-GQD	ROS neutralization[bf]	N-GQD	ROS Neutralization[bf]	GQD	ROS Neutralization[bf]
0	0	1.84±0.16	1.53±0.11	0.03±0.01	1.04±0.07	0.03±0.02	0.72±0.05	0.02±0.01

$O_2^{\bullet-}$ (by GSH)[g]								
Negative control[ag]	ROS neutralization[abg]	Positive Control[dg]	amino-N-GQD	ROS neutralization[bg]	N-GQD	ROS Neutralization[bg]	GQD	ROS Neutralization[bg]
0	0	96.2±4.2%	84.8±3.6%	0.4±0.2%	58.5±2.5%	0.3±0.1%	40.4±1.9%	0.3±0.2%

[a]Negative control: only treat reagent and laser irradiation without material (0 μg mL^{-1}).

[b]ROS neutralization: with the treatments of nanomaterial, the laser irradiation and 30 ppm of antioxidant α-tocopherol/methyl linoleate.

[c]SOSG reagent (Ex/Em: 488/525 nm) has a specific reactivity to generate fluorescence recorded by a PL spectrometer.

[d]Positive control: the treatment of 50 μM *tert*-butyl hydroperoxide (TBHP) and laser irradiation.

[e]*t*-MVP (Ex/Em: 352/465 nm) can react with $^1O_2$, forming a dioxetane intermediate that generates fluorescence upon decomposition to 1-pyrenecarboxaldehyde, and monitored by a PL spectrometer.

[f]XTT would interact with $O_2^{\bullet-}$ and produce the XTT-formazan generating strong absorption (470 nm in wavelength).

[g]GSH containing a thiol-tripeptide can prevent damages to cellular or bacterial components caused by stress of oxidation. Thiol group from GSH can be oxidized to disulfide bond converting GSH to glutathione disulfide. GSH oxidation was used to determine the generated $O_2^{\bullet-}$. Loss of GSH (%) = (absorbance difference between of sample and negative control / absorbance of negative control) × 100 %.

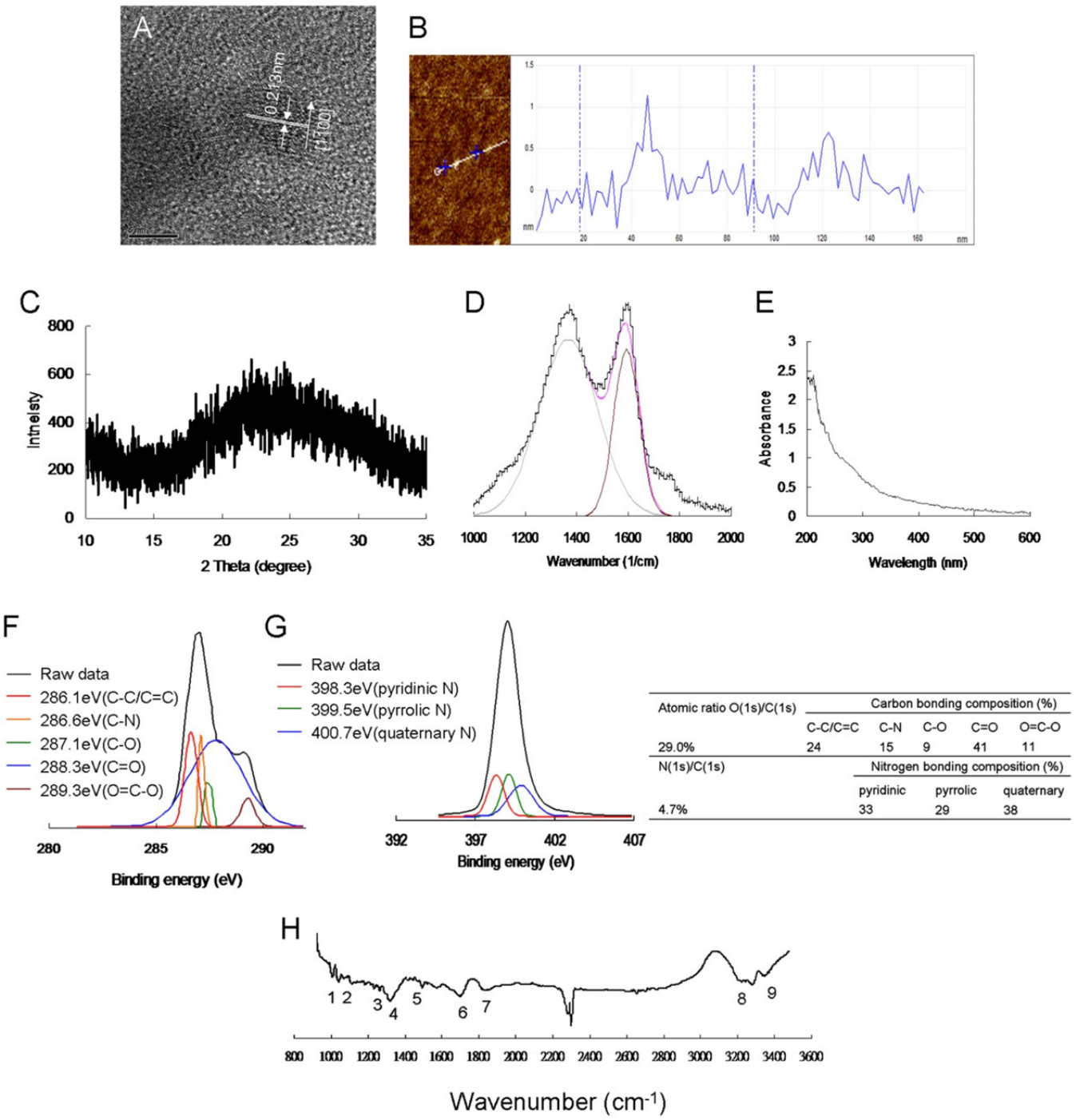

Atomic ratio O(1s)/C(1s)	Carbon bonding composition (%)				
	C-C/C=C	C-N	C-O	C=O	O=C-O
29.0%	24	15	9	41	11
N(1s)/C(1s)	Nitrogen bonding composition (%)				
	pyridinic	pyrrolic	quaternary		
4.7%	33	29	38		

Figure S3. (**A**) HR-TEM image derived for a single N-GQD, illustrating the graphene $\{1\bar{1}00\}$ lattice planes and the mean lateral size of 7.0 ± 0.4 nm with a *d*-spacing of 0.213 nm. (**B**) AFM image of N-GQDs on mica, and the height different between two arrows (the N-GQD and mica) was 1.05 ± 0.03 nm. (**C**) XRD pattern of N-GQDs. The diffraction angle of the N-GQD material was nearly $2\theta = 24.3°$, indicating appropriate layer regularity as well as a well-ordered lamellar structure exhibiting a 0.360-nm interlayer distance. (**D**) Raman spectroscopy for determining material's crystallinity. The gray and brown lines indicate that the spectrum was decomposed and fitted into the D-band (~1383 cm^{-1}) and G-band (~1608 cm^{-1}) peaks (black line: raw data; pink line: decomposed spectrum) with I_D/I_G integrated intensity

ratio of the D and G bands to be approximately 0.89. Additionally, the estimated size could also be obtained from the Raman calculations (~6.8 nm) was slightly lower because the Raman estimation (Eqs. S4-S5)[11-14] ignored the oxygenated regions. (**E**) UV-vis spectrum of material (222 nm corresponded to the π–π* transition of aromatic C=C bonds, and the n–π* transitions of the C–N and C=O shoulder appeared at approximately 323 nm). (**F-G**) Peaks that were fitted by employing a Gaussian function for the deconvoluted C(1s) of XPS spectra were as follows: nonoxygenated ring (C–C/C=C), C–N bonds, hydroxyl (C–O), carbonyl (C=O), and carboxylate (O=C-O); the N(1s) XPS spectra and fitted peaks using the Gaussian function were as follows: pyridinic N, pyrrolic N, and quaternary N, respectively. The atomic ratios and binding compositions for N-GQD are summarized in the table. O(1s)/C(1s) and N(1s)/C(1s) atomic ratios were 29.0% and 4.7%, respectively. (**H**) FTIR spectrum of material. The characteristic bands of N-GQDs were approximately for 1021 cm^{-1} of epoxy stretching (band 1); 1066 cm^{-1} of C—O stretching (band 2); 1238 cm^{-1} of phenolic C—OH (band 3); 1371 cm^{-1} of tertiary alcoholic C—OH bending (band 4); 1422 cm^{-1}, 1425 cm^{-1} and 1443 cm^{-1} of symmetric carboxylate C(=O)$_2^-$, sp^2 C=N and sp^3 C—N stretching (band 5); 1695 cm^{-1} of C=C ring stretching (band 6); 1828 cm^{-1} of C=O stretching (band 7); 3203 cm^{-1} of carboxylate O—H stretching (band 8); 3389 cm^{-1} of N—H in-plane stretching (band 9). Delivered dose of material: 6 μg mL^{-1}.

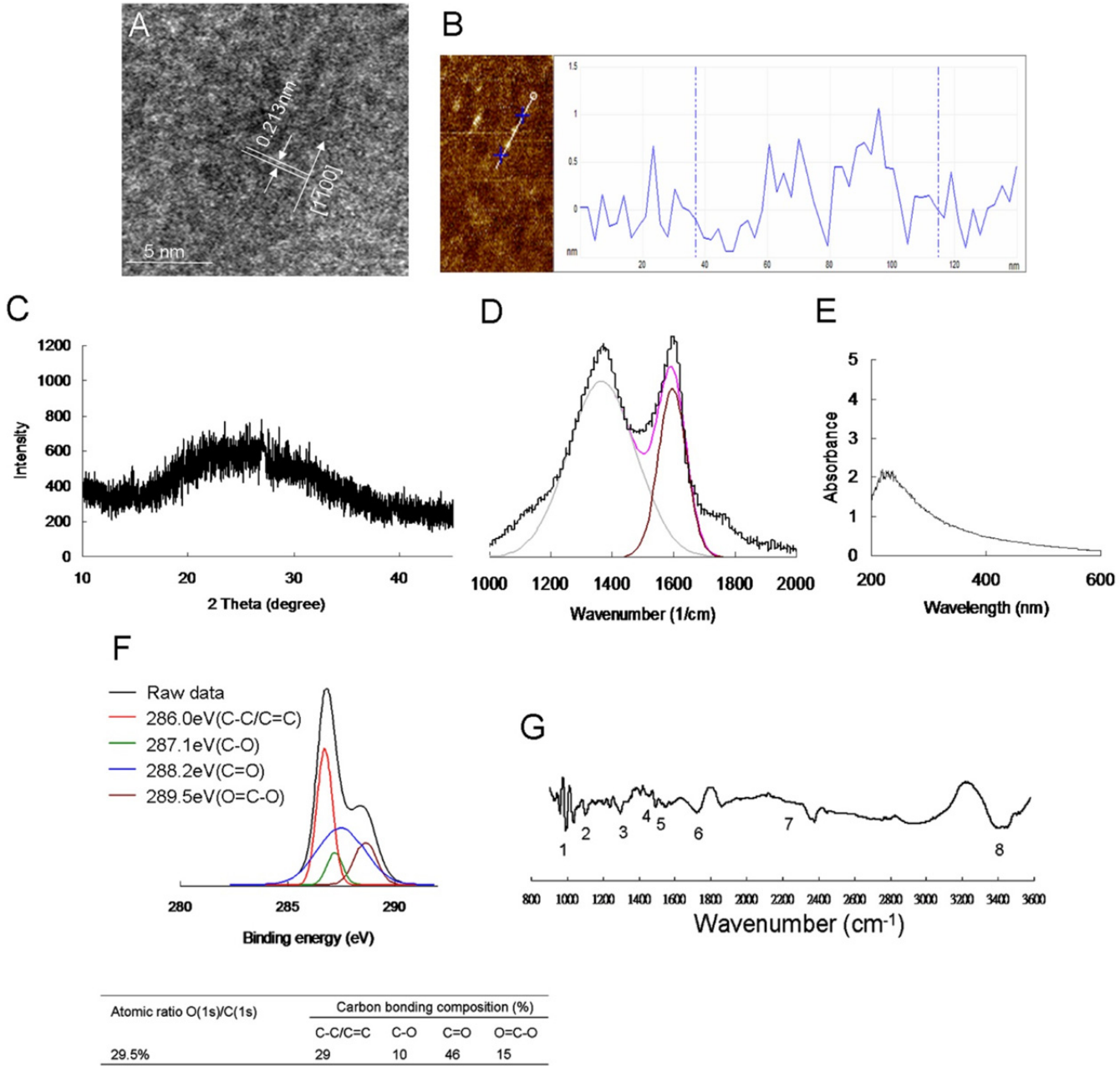

Atomic ratio O(1s)/C(1s)	Carbon bonding composition (%)			
	C-C/C=C	C-O	C=O	O=C-O
29.5%	29	10	46	15

Figure S4. (**A**) HR-TEM image derived for a single GQD, illustrating the graphene {1$\bar{1}$00} lattice planes and the mean lateral size of 6.8 ± 0.5 nm with a *d*-spacing of 0.213 nm. (**B**) AFM image of GQDs on mica, and the height different between two arrows (the GQD and mica) was 1.12 ± 0.04 nm. (**C**) XRD pattern of GQDs. The diffraction angle of the GQD material was nearly $2\theta = 24.3°$, indicating appropriate layer regularity as well as a well-ordered lamellar structure exhibiting a 0.360-nm interlayer distance. (**D**) Raman spectroscopy for determining material's crystallinity. The gray and brown lines indicate that the spectrum was decomposed and fitted into the D-band (~1385 cm^{-1}) and G-band (~1608 cm^{-1}) peaks (black line: raw data; pink line: decomposed spectrum) with I_D/I_G integrated intensity ratio of the D and G bands to be approximately 0.90. Additionally, the estimated size could also be obtained from the Raman calculations (~6.7 nm) was slightly lower because the Raman estimation (Eqs. S4-S5)[11-14] ignored the oxygenated regions. (**E**) UV-vis spectrum of material (224 nm corresponded to the π–π^* transition of

aromatic C=C bonds, and the n–π* transitions of the C=O shoulder appeared at approximately 322 nm). (**F**) Peaks that were fitted by employing a Gaussian function for the deconvoluted C(1s) of XPS spectra were as follows: nonoxygenated ring (C–C/C=C), hydroxyl (C–O), carbonyl (C=O), and carboxylate (O=C-O), respectively. The atomic ratio and binding compositions for GQD are summarized in the table. O(1s)/C(1s) atomic ratios were 29.5%. (**G**) FTIR spectrum of material. The characteristic bands of GQDs for epoxy stretching about 992 cm^{-1} (band 1), C–O stretching about 1071 cm^{-1} (band 2), tertiary alcoholic C–OH bending about 1360 cm^{-1} (band 3), symmetric carboxylate $C(=O)_2^-$ stretching about 1419 cm^{-1} (band 4), asymmetric carboxylate $C(=O)_2^-$ stretching about 1557 cm^{-1} (band 5), C=C ring stretching about 1706 cm^{-1} (band 6), broad O–H stretching about 2241 cm^{-1} (band 7), and cyclic alkanes, C–H stretching, intermolecular hydrogen bonded and O–H stretching about 3404 cm^{-1} (band 8). Delivered dose of material: 6 μg mL^{-1}.

The number of bacteria surviving by CFU assays after photoexcitation at a TPE power of 394.24 nJ pixel^{-1} with 700 scans (Ex: 800 nm; approximately 3.171 s of total effective exposure time) was performed by treating bacteria with materials-Ab_{TasA}-treated *B. subtilis* for 3 h of incubation at 37 ℃ in the dark. Amino-N-GQD-, N-GQD-, and GQD-Ab_{TasA}-treated *B. subtilis* exhibited approximately 7.875, 0.382 and 0.189 log10 reduction corresponding to nearly 0%, 42% and 65% viability (**Figure S5**).

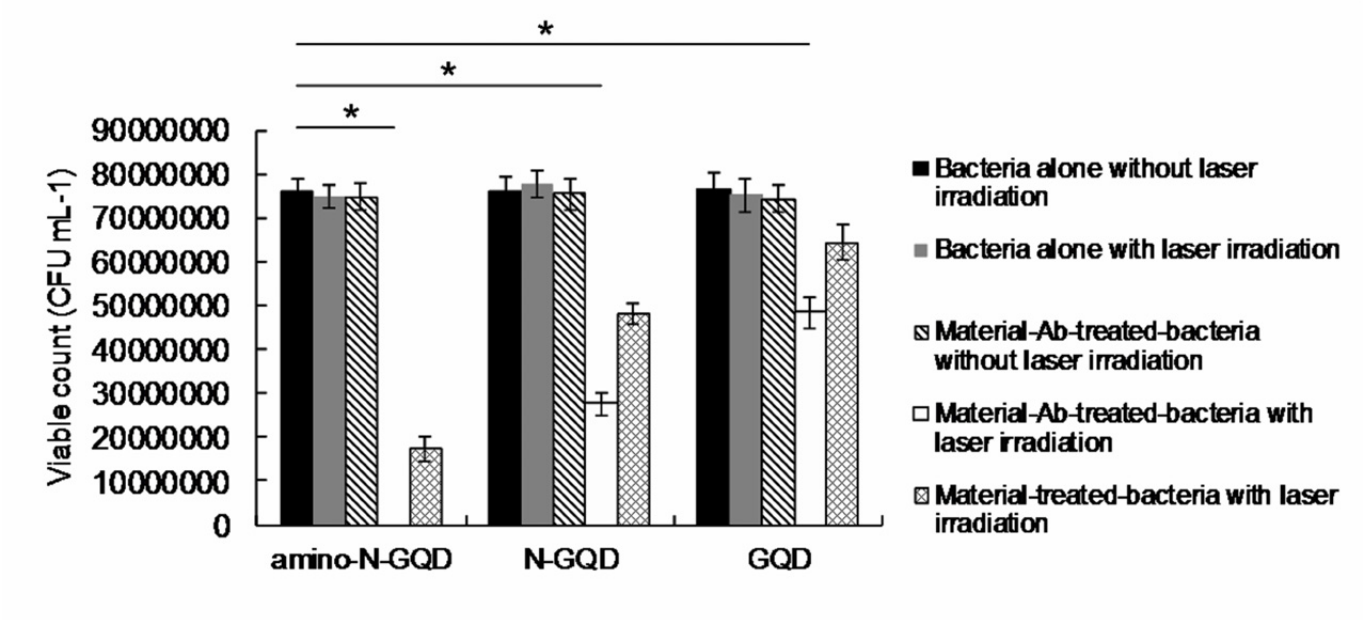

Figure S5. The number of surviving materials-Ab_{TasA}-treated *B. subtilis* was determined by CFU counting assay and are expressed as the percentage (%) that corresponds to the unit of CFU mL^{-1}. Delivered dose: OD_{600} ~ 0.05 of *B. subtilis* and 6 μg mL^{-1} material-Ab_{TasA}. Data are means ± SD (n=6). p< 0.0001, p= 0.0579 and p= 0.6211 for amino-N-GQD, N-GQD and GQD, respectively. *p value obtained by Student's t test.

The number of bacteria surviving by CFU assays after photoexcitation at the TPE of 394.24 nJ pixel^{-1}, 475.20 nJ pixel^{-1}, and 566.72 nJ pixel^{-1} (Ex: 800 nm; with 700 scans, approximately 3.171 s of total effective exposure time) was performed by treating bacteria with materials-Ab_{TasA}-treated *B. subtilis* for 3 h of incubation at 37 ℃ in the dark. Amino-N-GQD-, N-GQD-, and GQD-Ab_{TasA}-treated *B. subtilis* exhibited the complete reduction corresponding to kill almost all of bacteria (**Figure S6**).

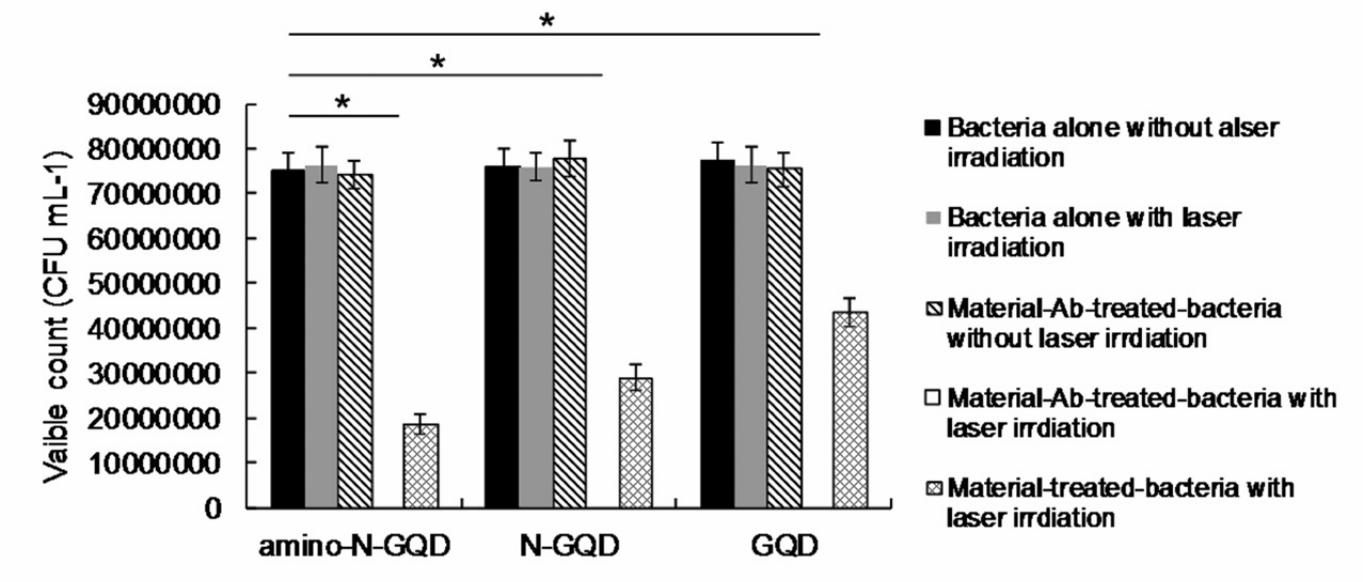

Figure S6. The number of surviving materials-Ab_{TasA}-treated *B. subtilis* was determined by CFU counting assay and are expressed as the percentage (%) that corresponds to the unit of CFU mL^{-1}. Delivered dose: OD_{600} ~ 0.05 of *B. subtilis* and 6 μg mL^{-1} material-Ab_{TasA}. Data are means ± SD (n=6). p< 0.0001 for all nanomaterials, respectively. *p value obtained by Student's t test.

Table S3. Amount of ROS generated, as observed by conducting TPE (394.24 nJ pixel^{-1}, 700 scans, Ex: 800 nm) on materials-Ab-treated-bacteria in the dark. The delivered dose of the materials was 6 μg mL^{-1}. Data are means ± SD (n = 6). [2,8-10,15-20]

$^1O_2$ (by SOSG)[c]								
Negative control[ac]	ROS neutralization[abc]	Positive Control[cd]	amino-N-GQD	ROS neutralization[bc]	N-GQD	ROS Neutralization[bc]	GQD	ROS Neutralization[bc]
225±10	226±11	2513±126	1499±104	227±15	878±61	226±10	532±27	225±12

$^1O_2$ (by *t*-MVP)[e]								
Negative control[ae]	ROS neutralization[abe]	Positive Control[de]	amino-N-GQD	ROS neutralization[be]	N-GQD	ROS Neutralization[be]	GQD	ROS Neutralization[be]
335±24	337±22	8056±198	4824±116	335±20	2791±73	334±23	1702±45	336±20

$O_2 \bullet^-$ (by XTT)[f]								
Negative control[af]	ROS neutralization[abf]	Positive Control[df]	amino-N-GQD	ROS neutralization[bf]	N-GQD	ROS Neutralization[bf]	GQD	ROS Neutralization[bf]
0	0	1.88±0.17	1.32±0.12	0.03±0.02	0.81±0.07	0.03±0.01	0.45±0.05	0.03±0.01

$O_2 \bullet^-$ (by GSH)[g]								
Negative control[ag]	ROS neutralization[abg]	Positive Control[dg]	amino-N-GQD	ROS neutralization[bg]	N-GQD	ROS Neutralization[bg]	GQD	ROS Neutralization[bg]
0	0	97.5±4.1%	80.9±3.0%	0.4±0.1%	48.3±2.5%	0.3±0.2%	30.3±1.9%	0.3±0.1%

[a]Negative control: only treat reagent and laser irradiation without material (0 μg mL^{-1}).

[b]ROS neutralization: with the treatments of nanomaterial, the laser irradiation and 30 ppm of antioxidant α-tocopherol/methyl linoleate.

[c]SOSG reagent (Ex/Em: 488/525 nm) has a specific reactivity to generate fluorescence recorded by a PL spectrometer.

[d]Positive control: the treatment of 50 μM TBHP and laser irradiation.

[e]*t*-MVP (Ex/Em: 352/465 nm) can react with $^1O_2$, forming a dioxetane intermediate that generates fluorescence upon decomposition to 1-pyrenecarboxaldehyde, and monitored by a PL spectrometer.

[f]XTT would interact with $O_2^{\bullet-}$ and produce the XTT-formazan generating strong absorption (470 nm in wavelength).

[g]GSH containing a thiol-tripeptide can prevent damages to cellular or bacterial components caused by stress of oxidation. Thiol group from GSH can be oxidized to disulfide bond converting GSH to glutathione disulfide. GSH oxidation was used to determine the generated $O_2^{\bullet-}$. Loss of GSH (%) = (absorbance difference between of sample and negative control / absorbance of negative control) × 100 %.

Table S4. Amount of ROS generated, as observed by conducting TPE (394.24 nJ pixel^{-1}, 700 scans; Ex: 800 nm) on materials-treated-bacteria in the dark. The delivered dose of the materials was 6 μg mL^{-1}. Data are means ± SD (n=6).[2,8-10,15-20]

$^1O_2$ (by SOSG)[c]								
Negative control[ac]	ROS neutralization[abc]	Positive Control[cd]	amino-N-GQD	ROS neutralization[bc]	N-GQD	ROS Neutralization[bc]	GQD	ROS Neutralization[bc]
223±8	225±10	2566±141	1112±193	225±9	540±82	227±11	203±35	224±10

$^1O_2$ (by *t*-MVP)[e]								
Negative control[ae]	ROS neutralization[abe]	Positive Control[de]	amino-N-GQD	ROS neutralization[be]	N-GQD	ROS Neutralization[be]	GQD	ROS Neutralization[be]
336±22	336±25	7929±181	4066±103	334±23	2039±52	335±22	686±45	337±21

$O_2^{\cdot-}$ (by XTT)[f]								
Negative control[af]	ROS neutralization[abf]	Positive Control[df]	amino-N-GQD	ROS neutralization[bf]	N-GQD	ROS Neutralization[bf]	GQD	ROS Neutralization[bf]
0	0	1.91±0.15	1.06±0.09	0.04±0.01	0.55±0.06	0.04±0.02	0.18±0.04	0.03±0.02

$O_2^{\cdot-}$ (by GSH)[g]								
Negative control[ag]	ROS neutralization[abg]	Positive Control[dg]	amino-N-GQD	ROS neutralization[bg]	N-GQD	ROS Neutralization[bg]	GQD	ROS Neutralization[bg]
0	0	98.0±4.5%	72.2±2.3%	0.3±0.2%	37.9±1.4%	0.4±0.1%	13.3±0.5%	0.4±0.2%

[a]Negative control: only treat reagent and laser irradiation without material (0 μg mL^{-1}).

[b]ROS neutralization: with the treatments of nanomaterial, the laser irradiation and 30 ppm of antioxidant α-tocopherol/methyl linoleate.

[c]SOSG reagent (Ex/Em: 488/525 nm) has a specific reactivity to generate fluorescence recorded by a PL spectrometer.

[d]Positive control: the treatment of 50 μM TBHP and laser irradiation.

[e]*t*-MVP (Ex/Em: 352/465 nm) can react with $^1O_2$, forming a dioxetane intermediate that generates fluorescence upon decomposition to 1-pyrenecarboxaldehyde, and monitored by a PL spectrometer.

[f]XTT would interact with $O_2^{\cdot-}$ and produce the XTT-formazan generating strong absorption (470 nm in wavelength).

[g]GSH containing a thiol-tripeptide can prevent damages to cellular or bacterial components caused by stress of oxidation. Thiol group from GSH can be oxidized to disulfide bond converting GSH to glutathione disulfide. GSH oxidation was used to determine the generated $O_2^{\cdot-}$. Loss of GSH (%) = (absorbance difference between of sample and negative control / absorbance of negative control) × 100 %.

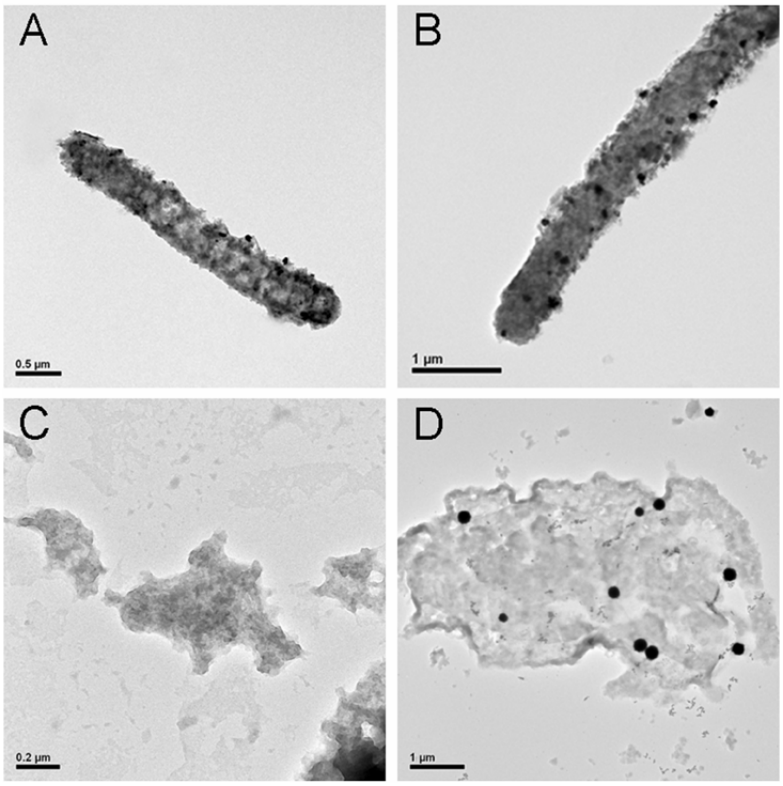

Figure S7. TEM images for *B. subtilis* (**A**) with GQD–Ab_{TasA}, (**B**) N-GQD–Ab_{TasA} and incubated for 3 h. Given a TPE power of 394.24 nJ $pixel^{-1}$ (scanning frequency, 700 scans; total effective exposure time, ~3.171 s; Ex, 800 nm), TEM images of the photoexcited– (**C**) N-GQD–Ab_{TasA}– (**D**) N-GQD–Ab_{TasA}– treated bacteria (3 h of incubation) Delivered dose: OD_{600}–0.05 for *B. subtilis* and 6 µg mL^{-1} for material–Ab_{TasA}.

In **Figure S8**, the amino-N-GQD-Ab_{TasA}-treated *B. subtilis* demonstrated no exceptional morphology after 3 h of incubation, whereas an incubation period of 3 d about to change the bacteria's shape (**Figure 3C**), corresponding to nearly 68% viability (**Figure 4B**).

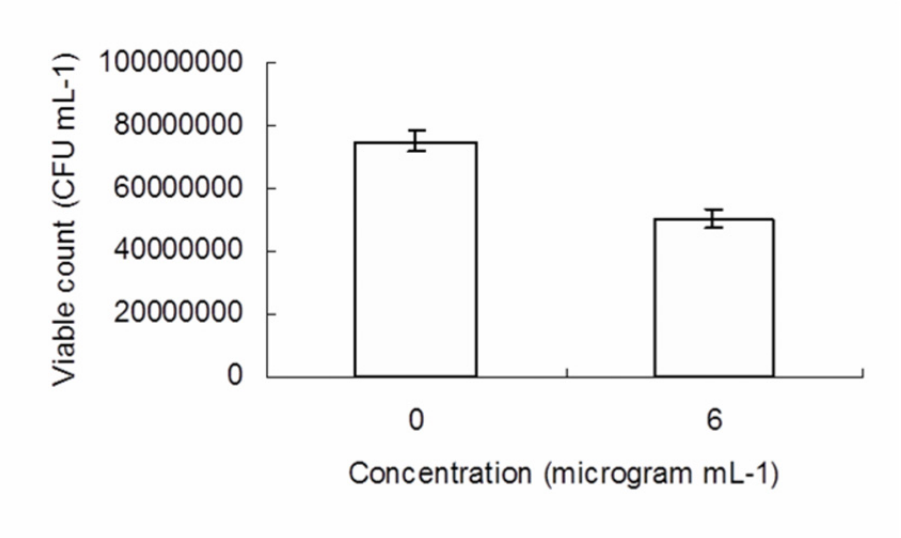

Figure S8. The number of surviving amino-N-GQD-Ab_{TasA}-treated *B. subtilis* was determined by CFU counting assay and are expressed as the percentage (%) that corresponds to the unit of CFU mL^{-1}. Delivered dose: OD_{600} ~ 0.05 of *B. subtilis* and 6 μg mL^{-1} amino-N-GQD–Ab_{TasA}. Data are means ± SD (*n*=6).

Table S5. Two-photon action cross sections of fluorescein (in 0.1 M NaOH, pH 11) and rhodamine B (in methanol). Excitation wavelength: 800 nm.

	Fluorescein (in ddH_2O, pH=11)	Action cross-section (ησ)
Excitation wavelength at 800 nm action cross section, $\eta\sigma_2$ (GM, $10^{-50}cm^4s$/photon)	35.8	154.2

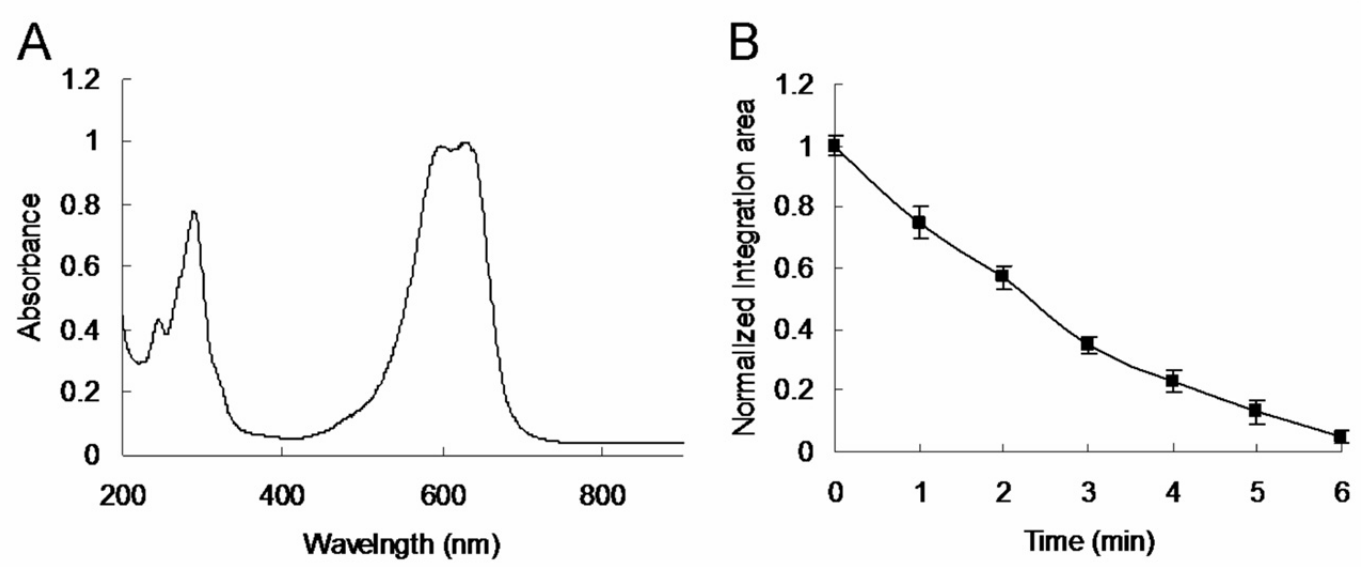

Figure S9. Two-photon stability. (**A**) UV-vis spectrum for the conventional photosensitizer, toluidine blue O/ ddH_2O. The absorbance at 633 nm was detected. (**B**) As a function of irradiation time (0−6 min) at a power density of 0.1 W cm^{-2} (Ex: 670 nm), the relative intensity of integrated area from 400 to 800 nm in wavelength of absorbance was calculated. Data are means ± SD (*n*=6).

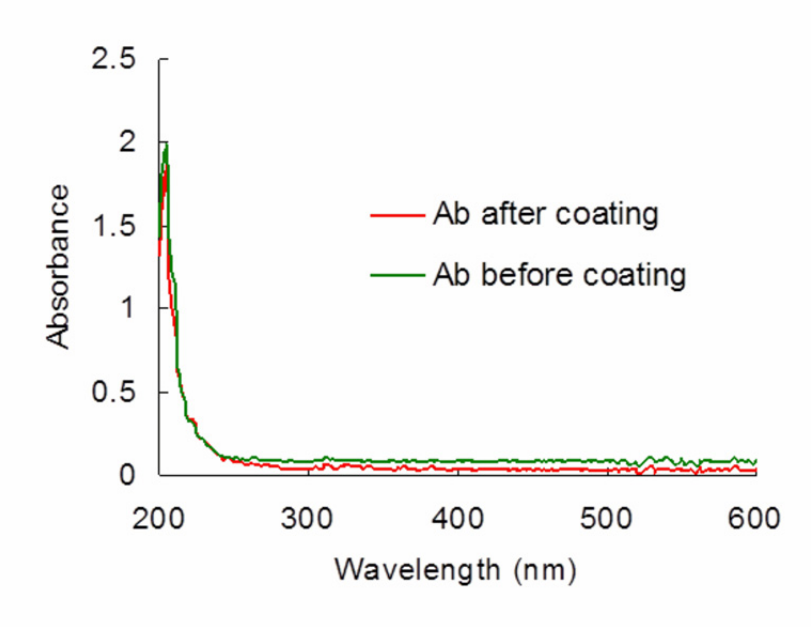

Figure S10. The absorbance of a quantity of antibody before/after coating was recorded *via* UV-vis spectroscopy (Abs: approximately 203 nm), respectively.

Table S6. Antibody coating efficiency and zeta potential of materials.

	1X PBS	Culture medium of *B. subtilis*
Amino-N-GQD-Ab_{TasA}	14.0%/ 16.3 mV	13.8%/ 16.0 mV
N-GQD-Ab_{TasA}	12.6%/ 15.2 mV	13.0%/ 15.4 mV
GQD-Ab_{TasA}	11.4%/ 10.2mV	11.7%/ 10.6 mV

References

1. Hummers WS, Offeman RE. Preparation of graphitic oxide. *J Am Chem Soc.* 1958;80:1339.

2. Kuo WS, Hsu CLL, Chen HH, et al. Graphene quantum dots conjugated with polymers for two-photon properties under two-photon excitation. *Nanoscale.*2016;8:16874–16880.

3. Teng, CY, Nguyen BS, Yeh, TF, et al. Roles of nitrogen functionalities in enhancing the excitation-indenpendent green-color photoluminescence of graphene oxide dots. *Nanoscale.* 2017;9:8256–8265.

4. Umezawa K, Matsui A, Nakamura Y, et al. Bright, color-tunable fluorescent dyes in the vis/NIR region: establishment of new "tailor-made" multicolor fluorophores based on borondipyrromethene. *Chem Eur J.* 2009;15:1096–1106.

5. Shi L, Hernandez B, Selko M. Singlet oxygen generation from water-soluble quantum dot-organic dye nanocomposites. *J Am Chem Soc.* 2006;128:6278–6279.

6. Xu C, Zipfel W, Shear JB, et al. Multiphoton fluorescence excitation: new spectral windows for biological nonlinear microscopy. *Proc Natl Acad Sci USA.* 1996;93:10763–10768.

7. Albota MA, Xu C, Webb WW. Two-photon fluorescence excitation cross Sections of biomolecular probes from 690 to 960 nm. *Appl Opt.* 1998; 37: 7352–7356.

8. Kinen MM, Kamal-Eldin A, Lampi AM, et al. Effects of α- and γ-tocopherols on formation of hydroperoxides and two decomposition products from methyl linoleate. *J Am Oil Chem Soc.* 2000;177:801–806.

9. Possel H, Noack H, Augustin W, et al. An oxidant, *tert*-butyl hydroperoxide (TBHP), to serve as a positive control. *FEBS Lett.* 1997;416:175–178.

10. Thompson A, Lever JR, Canella KA, et al. Chemiluminescence mechanism and quantum yield of synthetic vinylpyrene analogues of benzo[*a*]pyrene-7,8-dihydrodiol. *J Am Chem Soc.* 1986;108:4498–4504.

11. Ferrari AC, Basko DM. Raman spectroscopy as a versatile tool for studying the properties of graphene. *Nat Nanotechnol.* 2013;8:235–246.

12. Tuinstra F, Koenig JL. Raman spectrum of graphite. *J. Phys. Chem.* 1970;53:1126–1130.

13. Pimenta MA, Dresselhaus G, Dresselhaus MS, et al. Studying disorder in graphite-based systems by Raman spectroscopy. *Phys Chem Chem Phys.* 2007;9:1276–1290.

14. Ferrari AC, Robertson J. Interpretation of Raman spectra of disordered and amorphous carbon. *Phys Rev B.* 2000;61:14095–14107.

15. Sharma P, Jha AB, Dubey RS, et al. Reactive oxygen species, oxidative damage, and antioxidative defense mechanism in plants under stressful conditions. *J Bot.* 2012;2012:1–26.

16. Chang WT, Chen SJ, Chang CY, et al. Effect of size-dependence photodestructuve efficacy by gold nanomaterials with multiphoton laser. *ACS Appl Mater Interfaces.* 2015;7:17318–17329.

17. Ellman GL. Tissue sulfhydryl gropus. *Arch Biochem Biophys.* 1959;82:70–77.

18. Carmel-Hare O, Storz G. Roles of the glutathione- and thioredoxin-dependent reduction systems in the *Escherichia coli* and *Saccaromyces cerevisiae* responses to oxidative stress. *Annu Rev Microbiol.* 2000;54:439–461.

19. Wu PC, Wang JY, Wang WL, et al. Efficient two-photon luminescence for cellular imaging using

biocompatible nitrogen-doped graphene quantum dots conjugated with polymers. *Nanoscale.* 2018;10:109–117.
20. Feng X, Li X, Li Z, et al. Size-dependent two-photon absorption in circular graphene quantum dots. *Opt Express.* 2016;24:2877−2884.